Polymer-$BaTiO_3$ Composites: Dielectric Constant and Vapor Sensing Properties in Chemocapacitor Applications

Kyriaki Manoli,[1,2] Petros Oikonomou,[1] Evangelos Valamontes,[3] Ioannis Raptis,[1] Merope Sanopoulou[2]

[1]*Institute of Microelectronics, National Center for Scientific Research "Demokritos", 15310 Ag. Paraskevi Attikis, Greece*
[2]*Institute of Physical Chemistry, National Center for Scientific Research "Demokritos", 15310 Ag. Paraskevi Attikis, Greece*
[3]*Electronics Engineering Department, Technological Educational Institute of Athens, Ag. Spiridonos 22, Egaleo, Greece*

Received 5 April 2011; accepted 27 July 2011
DOI 10.1002/app.35362
Published online 29 January 2012 in Wiley Online Library (wileyonlinelibrary.com).

ABSTRACT: In this work, composite materials, prepared by inclusion of various amounts of $BaTiO_3$ nanoparticles in PBMA and PHEMA polymer matrices, were characterized in respect to their dielectric properties and then used as the sensing layer of capacitive-type sensors. $BaTiO_3$ was found to be less effective in enhancing the permittivity of PHEMA, as compared to PBMA, in the range of 1 kHz–1 MHz, possibly due to the observed lower quality of dispersion in the polymer matrix and the higher polarity of the polymer in the former case. The response of the composite-based chemocapacitors to four vapor analytes, covering a wide range of dielectric constants, was studied in relation to the $BaTiO_3$ load. In all cases, with increasing amount of $BaTiO_3$ load, the absolute value of capacitance response was increased, due to the corresponding increase of the initial capacitance of the sensing composite layer. However, the corresponding normalized (to the initial capacitance of the sensing composite layer) capacitance values were reduced, due to the decreased volume fraction of the sorbing polymer material in the composite matrix. An exception to this trend, observed upon exposure of the PBMA/$BaTiO_3$ chemocapacitors to low humidity levels, is also presented and discussed. J Appl Polym Sci 125: 2577–2584, 2012

Key words: nanocomposites; dielectric properties; sensors; barium titanate; capacitive sensors

INTRODUCTION

The range of polymer applications is continuously expanding thanks to the modification/improvement of their properties by inclusion of micro-, or nano-, sized fillers to meet specific technological needs. To overcome the low dielectric permittivity of most organic polymers, which constitutes a drawback in many electronic applications, polymer composites loaded with high dielectric permittivity materials, such as the perovskite-type $BaTiO_3$ oxide, are employed. As all analogous material properties of two-phase systems, the dielectric properties of polymer-$BaTiO_3$ composites depend on the size, shape and volumetric fraction of the embedded $BaTiO_3$ particles, the efficiency of their dispersion in the polymer matrix, and the properties of the host polymer. Such composites are actively investigated as passive components in electronic systems.[1–4] They have also been employed in sensor applications,[5–8] mainly for humidity monitoring,[6–8] since porous or nanocrystalline $BaTiO_3$ is known to increase its surface conductivity and dielectric constant in the presence of water.[9,10]

The principle of operation of polymer-based chemical sensors for the quantitative detection of volatile organic compounds (VOCs) or humidity, relies on the changes of a physicochemical property of the polymer due to analyte absorption, as for example in resistive-type[11] or capacitive-type[6] sensors. Capacitive-type gas sensors are attractive devices due to their processability, low fabrication cost, reversibility and the wide range of polymeric material choice. On the other hand, with the ever-increasing demand for miniaturization of electronic devices, the low dielectric constant of polymers may be a critical technological issue in terms of reliable capacitance measurements, especially those concerning the detection limit for a specific target analyte or the discriminating ability of the sensor towards gas mixtures. In this respect, the incorporation of high-k materials in the polymeric sensing layer may improve the sensor's performance.

In this work, composite materials prepared by incorporation of various amounts of $BaTiO_3$ in poly(2-hydroxyethyl methacrylate) (PHEMA) and poly(*n*-butyl methacrylate) (PBMA) polymer matrices

Correspondence to: M. Sanopoulou (sanopoul@chem.demokritos.gr).

were characterized in terms of their dielectric permittivity and then used as sensing layers in microfabricated interdigitated capacitive (IDC) sensors for the detection of four vapor analytes covering a wide range of dielectric constants: water, methanol, ethanol, and ethyl acetate. The responses of the chemocapacitors to these vapor analytes was studied in relation to the $BaTiO_3$ load and the possible interactions between analyte, polymer, and $BaTiO_3$ particles.

EXPERIMENTAL

Poly(2-hydroxyethyl methacrylate) [PHEMA] ($M_w \sim$ 300 K; d (25°C): 1.15 g/mL; T_g: 109°C) and poly (*n*-butyl methacrylate) [PBMA] ($M_w \sim$ 337 K; d (25°C): 1.07 g/mL; T_g: 15°C) in the form of powder, and $BaTiO_3$, with an average particle size $<$ 100 nm and d (25°C): 6.08 g/mL, were purchased from σ-Aldrich. Propylene glycol methyl ether acetate (PGMEA), ethyl lactate, ethanol (EtOH), methanol (MeOH), and ethyl acetate (AcOOEt), all of analytical reagent grade, were also purchased from σ-Aldrich and used without further purification.

Pure polymer layers were prepared by casting 6–10% w/w ethyl lactate solutions of PHEMA and 10% w/w PGMEA solutions of PBMA. For the preparation of composite layers, $BaTiO_3$ was at first ball milled for 5 h and dispersed, ultrasonically for 3 h, to the solvent used for each polymer (20% w/w in ethyl lactate or PGMEA). The $BaTiO_3$ dispersions were then mixed with the corresponding polymer–solvent solutions at appropriate ratios, and magnetically stirred for 24 h before casting on the Al electrodes of the IDC sensors, or on Al substrates for the dielectric constant determination, or on glass substrates for optical characterization.

IDC sensors were fabricated from Al electrodes on 4 in. Quartz wafers by applying conventional microelectronic processes. In particular a 300 nm thick aluminum layer is deposited on the quartz wafer using e-gun evaporation, which is then patterned with standard optical lithography and wet etching to form a 4-IDC sensor array per chip. The geometrical characteristics of each sensor are the nominal width of each finger $w = 5$ μm, the distance between adjacent fingers $g = 5$ μm [metallization ratio $\eta = w/(w + g) = 0.5$, spatial wavelength $\lambda = 2(w + g) = 20$ μm]. The sensing area of each IDC structure is 4 mm × 4 mm, with a total number of fingers $N = 400$. The polymer/$BaTiO_3$ films were applied on the sensing area by drop casting.

Optical microscopy studies, at reflectance mode, of films deposited on glass substrates were performed with a Olympus MX51 optical microscope equipped with a Olympus DP71 camera.

For the dielectric constant determination, vertical capacitors were fabricated starting from Al substrate followed by deposition of the composite polymeric film and finally by the Al deposition of the second capacitor plate through a Si shadow mask that has been prepared by standard micromachining processing. The dielectric constant of the composite film, was calculated from capacitance measurements in the range 1 kHz–1 MHz, by the use of an impedance bridge LCR HP 4192A, in conjunction with the area of the Al electrodes (0.0192–0.0292 mm^2), accurately calculated through image processing and structure measurement of appropriate optical microscope images, and the thickness of the films (350–1000 nm) as determined by stylus profilometry.

Evaluation of the sensors regarding their response to the presence of particular analytes was performed in a small volume ($\sim$ 4 cm^3) chamber thermostated at 30 ± 0.1°C. In the gas-delivering unit a dry nitrogen flux is initially split in a carrier and a diluting part with the help of mass flow controllers. The desired analyte concentration is generated by mixing nitrogen with saturated analyte vapor at 30°C and at atmospheric pressure.[12] The mixture passes through the sample chamber continuously at a rate of 1000 L/min. All components of the gas delivering unit, and the capacitance meter (HP 4278A), are controlled by a dedicated software developed on the LabView platform. Capacitance measurements were performed in the range 1 kHz–1 MHz.

RESULTS

Optical characterization and dielectric constant of composite materials

In Figure 1, typical top-down optical micrographs of composite layers deposited on glass substrates are presented. The $BaTiO_3$ particles appear more homogeneously dispersed in the PBMA matrix with the majority of roughly spherical aggregates having diameter $\leq$ 2 um. In contrast, in the PHEMA matrix, irregularly shaped aggregates with a long dimension of up to $\sim$ 6 um are observed. This difference between the two matrices may be partly attributed to the lower surface tension of solvent PGMEA (used for the PBMA-based layers) as compared to ethyl lactate (used for the PHEMA-based layers), resulting in better wetting of the nanoparticles by the former solvent and thus smaller agglomerates in the PBMA matrix.

The dielectric constants of pure polymer (ε_p), and of composite (ε_c), layers, from the vertical capacitor measurements, were determined in the 1 kHz–1 MHz range. In all cases, with increasing frequency a mild drop of the dielectric constant was observed. The results for the PHEMA-based materials are shown in Figure 2. The ε_c versus frequency plots of the composites have similar slopes with that of pure

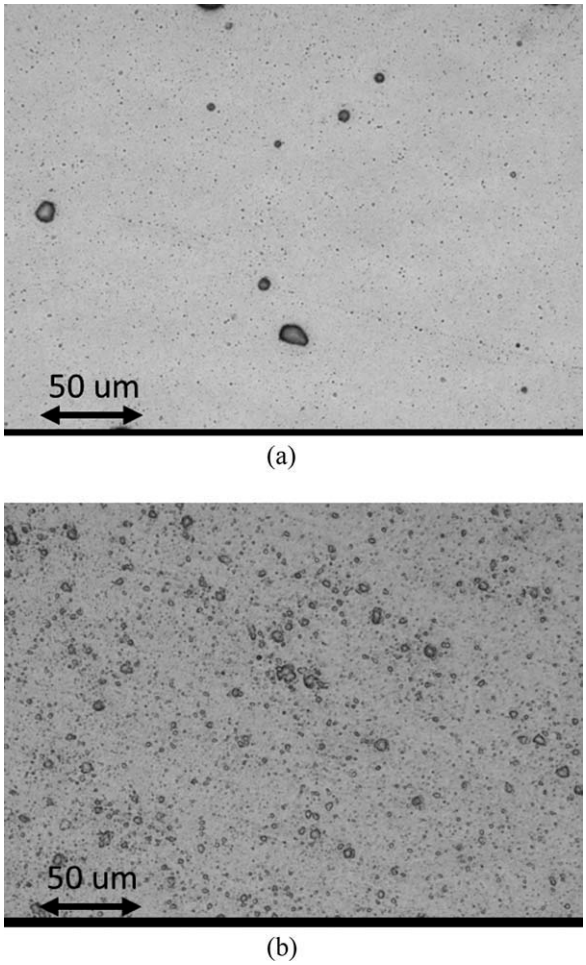

Figure 1 Optical micrographs of 10% v/v $BaTiO_3$-loaded PBMA (a) and PHEMA (b) layers, deposited on glass substrates.

PHEMA, as also found for other polymer/$BaTiO_3$ systems in this frequency range and attributed mainly to dielectric relaxations of the polymer matrix.[13] Similar frequency-dependent behavior was found for PBMA/$BaTiO_3$ composites. However, low frequency measurements were associated with higher noise; accordingly, a detailed analysis of the results at 1 MHz is presented below.

The dielectric constant, at 1 MHz, of pure polymer layers was found to be 2.89 ± 0.06 for PBMA and 10.49 ± 0.29 for PHEMA. With increasing $BaTiO_3$ load in the layer, the dielectric constant of the composite increased. For a certain load, the value of the composites dielectric constant, ε_c, was higher in the case of PHEMA matrix as compared to PBMA one, due to the higher dielectric constant ε_p of the pure polymer in the former case. However, a stronger dependence of the normalized increase, $\varepsilon_c/\varepsilon_p$, on the volume fraction, ϕ_f, of embedded $BaTiO_3$ was found for PBMA composites, as shown in Figure 3. Experimental studies indicate that the quantitative dependence of ε_c on the volume fraction of $BaTiO_3$ may

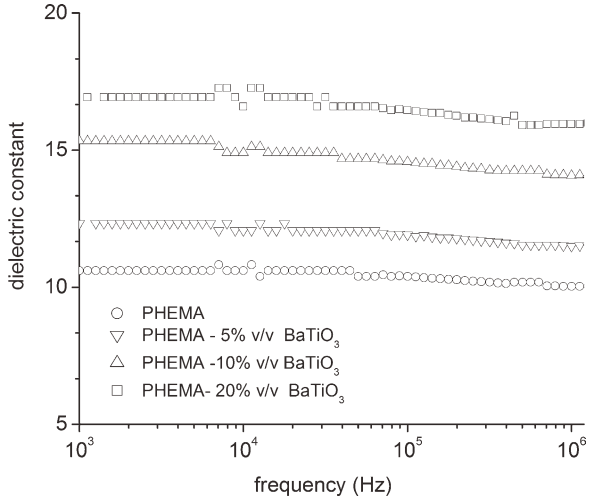

Figure 2 Dielectric constant of pure PHEMA and PHEMA/$BaTiO_3$ composites as a function of frequency.

vary according to the host polymer used.[13–15] From the theoretical point of view, various mixing rules have been proposed for the functional dependence of ε_c on the filler volume fraction, ϕ_f. According to the Maxwell model, the permittivity of the composite material and is given by[16]:

$$\frac{\varepsilon_c}{\varepsilon_p} = 1 + 3\phi_f \left[\frac{\left(\frac{\varepsilon_f}{\varepsilon_p} + 2\right)}{\left(\frac{\varepsilon_f}{\varepsilon_p} - 2\right)} - \phi_f \right]^{-1} \quad (1)$$

Equation (1) has been developed for relatively low volume fractions φ_f of spherical particles,

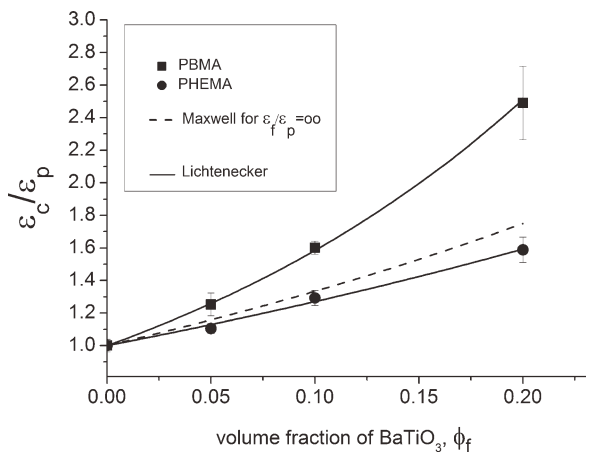

Figure 3 Dependence of the normalized dielectric constant, $\varepsilon_c/\varepsilon_p$, of composites based on PHEMA (circles) and PBMA (squares) on the volume fraction of embedded $BaTiO_3$ particles. Error bars represent standard error of mean experimental values, derived from three samples. Measurements performed at 1 MHz. Solid lines represent fitting of eq. (2) to experimental data and dotted line represents the upper limit predictions of eq. (1).

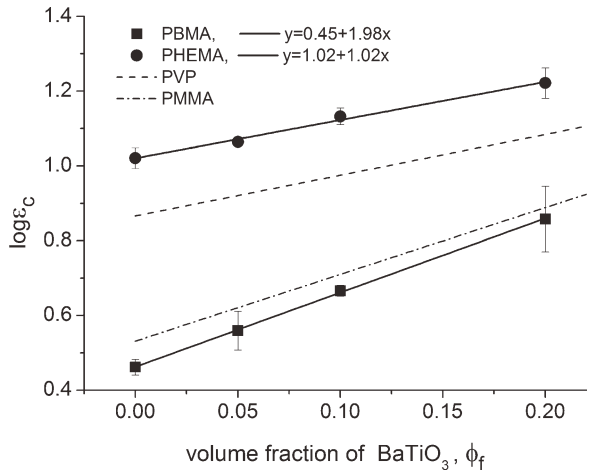

Figure 4 Semilogarithmic plot of data of Figure 3 for composites based on PHEMA (circles) and PBMA (squares), and corresponding fitting to eq. (2) (solid lines). Dashed and dotted-dashed lines represent experimental data for the $BaTiO_3$/PVP and $BaTiO_3$/PMMA systems, taken from Refs. 21 and 22, respectively.

characterized by dielectric constant ε_f, homogenously dispersed in the polymer phase characterized by dielectric constant ε_p, and has been also applied for other properties of composite materials.[16,17] The upper limit of $\varepsilon_c/\varepsilon_p$ predicted by eq. (1) (for $\varepsilon_f/\varepsilon_p \rightarrow \infty$), shown in Figure 3 as dotted line, falls well below the experimental data for the PHEMA-$BaTiO_3$ composites as it was also reported for epoxy-$BaTiO_3$ composites.[18] An alternative mixing rule, found in many cases applicable to the permittivity of ceramics/polymer composites, is the Lichtenecker logarithmic expression[4,13,14,19,20]

$$\log \varepsilon_c = (1 - \phi_f) \log \varepsilon_p + \phi_f \log \varepsilon_f \qquad (2)$$

As shown in Figure 4, the experimental data of the two polymer-filler systems studied here, follow the linear relation between log ε_c and the volume fraction ϕ_f of the filler, predicted by eq. (2). The slope of the plots, in conjunction with the y-intercept, provided an effective value of ε_f, for each system. The higher ε_f value derived for the PBMA composites ($\varepsilon_f = 275$) as compared to the PHEMA ones ($\varepsilon_f = 110$), quantifies the stronger effect of $BaTiO_3$ particles in the former case, noted above. Possible reasons for this differentiation between the two polymer systems are (i) the less effective dispersion of the filler in PHEMA (see Fig. 1) resulting in larger aggregates and poorer wetting by the polymer phase and consequently air-filled voids in the composite matrix,[18] and (ii) to the higher polarity of PHEMA. According to refs[13,14] the dielectric losses of a polymer matrix in the MHz-GHz frequency range increase with increasing polarity of the matrix, and the effect is more pronounced in the case of embedded high-k particles, such as $BaTiO_3$. This interpretation is supported from literature data for $BaTiO_3$ composites based on polyvinylpyrrolidone (PVP)[21] and poly (methyl methacrylate) (PMMA),[22] included in Figure 4. In particular, the slope of the logε_c versus ϕ_f plot for the polar PVP ($\varepsilon_p \sim 7$) is close to that of PHEMA, in contrast to the slope of the less polar PMMA ($\varepsilon_p \sim 3.4$) which is close to that of PBMA.

The pure polymers and the corresponding composite materials with 10 and 20%v/v $BaTiO_3$ load were subsequently used for the construction, characterization and evaluation of IDC sensors, as described below.

Initial capacitance of sensors based on composite materials.

Results on the capacitance of the sensing composite layer (C_c) of IDC sensors based on PBMA and PHEMA, at 1 kHz, are shown in Figure 5. The value of C_c is derived by substracting the measured capacitance of the bare electrodes (C_{sub}) from that after deposition of the sensing layer (C_0), under pure nitrogen flow. The dependence of C_c on ϕ_f bears the same characteristics with the corresponding results for ε_c (Fig. 4), i.e., (i) C_c values for a certain ϕ_f are higher for the PHEMA-based composite, due to the higher C_p of PHEMA (ii) for both type of polymer matrices there is a linear relation between log C_c and ϕ_f, and (iii) the slope of the log C_c versus ϕ_f plot is higher for the less polar PBMA. Thus, on a quantitative basis, pure PBMA layers are characterized by $C_p \sim 11$ pF and a maximum increase by a factor of ~ 3 upon inclusion of 20% v/v $BaTiO_3$, while the C_p value for pure PHEMA layers is ~ 40 pF and a twofold increase was observed by 20% v/v $BaTiO_3$ load.

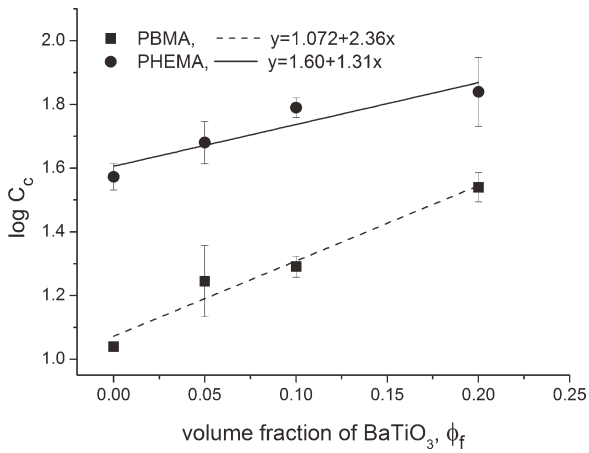

Figure 5 Semilogarithmic plot of the initial capacitance C_c, at 1 KHz, of the sensing composite layer of IDC sensors based on PHEMA (circles) and PBMA (squares) versus the volume fraction of embedded $BaTiO_3$ particles. Error bars represent standard error of mean experimental values, derived from three samples.

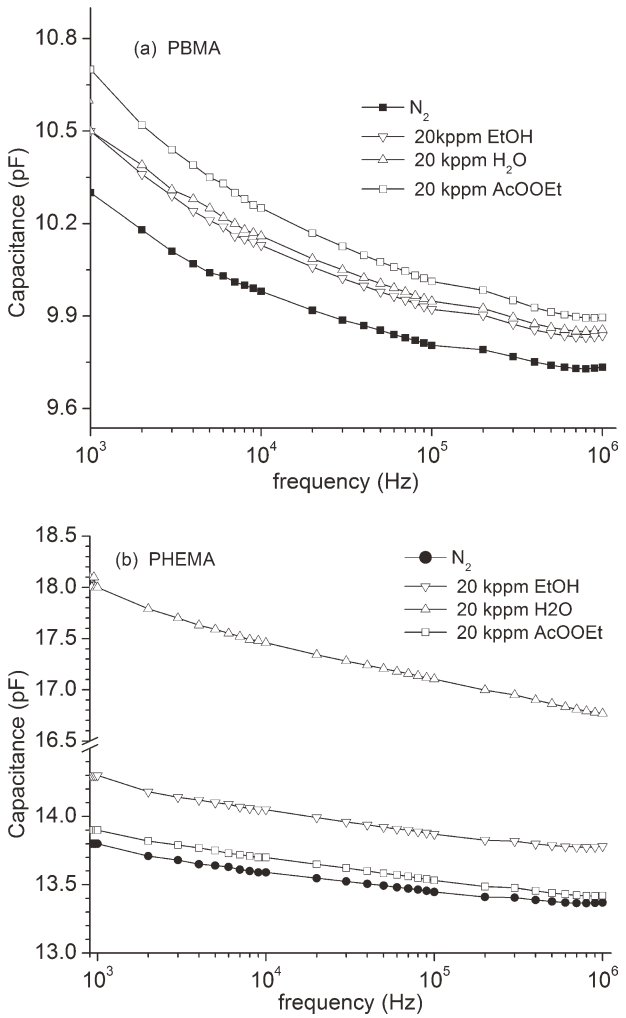

Figure 6 Frequency-dependence of capacitance responses of pure PBMA-based (a) and pure PHEMA-based (b), sensors exposed to pure N_2 flow and to 20kppm of ACOOEt, EtOH, and H_2O. The sensing area of the particular IDCs was 1 mm × 1 mm.

Dependence of sensor responses on the frequency of measurement

The effect of frequency was studied in the case of pure polymer chemocapacitors, exposed to pure N_2 flow and to 20 kppm of ACOOEt, EtOH, and H_2O. (Fig. 6(a,b)]. In line with the results on the dielectric constant, in the 1 kHz–1 MHz range, the sensor's capacitance (C_0) under N_2 flow decreases with increasing frequency, with an overall drop of ~ 3% for the PBMA-based sensor and ~ 5% for the PHEMA-based one. Analogous frequency-dependent behavior was also found in the presence of the three analytes, for both sensors, indicating that the observed decrease of capacitance with increasing frequency is primarily due to the relaxations of the polymer matrix. Similarly moderate drops of capacitance were observed in the same frequency range and at ambient temperatures for other polymeric materials and polymer–organic vapor systems.[23,24] Although the drop in capacitance responses is small in the measured frequency range, we chose the 1 KHz frequency for subsequent studies. However, we note that possible differences in the frequency-dependence of the responses of specific sensing layers, swollen by different analytes, may provide useful information for the discrimination of analytes by capacitance measurements at different frequencies.[23,25]

Effect of $BaTiO_3$ load on the responses of PHEMA-based sensors

The capacitance changes, ΔC of a pure PHEMA sensor, as well as of PHEMA-$BaTiO_3$ sensors with two different $BaTiO_3$ loads (10 and 20% v/v), in the presence of 5000 ppm of ACOOEt, EtOH, MeOH, and H_2O, are shown in Figure 7. The change ΔC of the pure-PHEMA sensor due to the corresponding changes in the dielectric constant of the polymeric layer are determined by the amount of analyte sorbed in conjunction with the latter's dielectric constant. The sorptive capacity of various polymeric materials, in the form of thin supported films, towards the four analytes studied here, has been previously determined by an optical methodology.[26] On the basis of the deduced polymer-analyte Flory-Huggins interaction parameters, at a given analyte activity, sorption in pure PHEMA films was found to follow the order AcOOEt≪H_2O<EtOH<MeOH. Taking into account that the concentration of 5000 ppm corresponds to activities lower than 0.1 for MeOH, EtOH and AcOOEt and ~ 0.15 for H_2O, the data of Figure 7 for the pure PHEMA sensor can be rationalized on the basis of the relative amount of each analyte sorbed at 5000 ppm in conjunction with the analyte's dielectric constant ε_s. Thus, the lowest

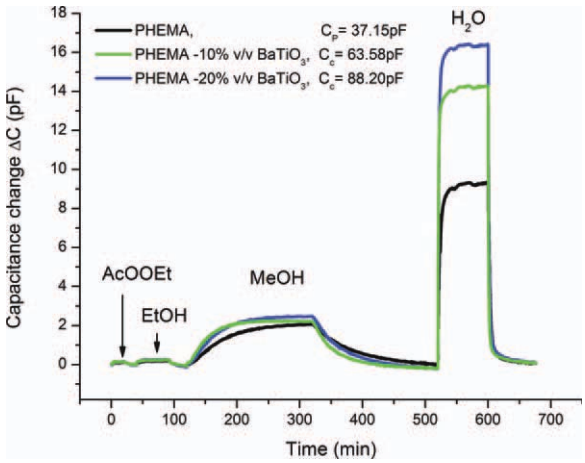

Figure 7 Effect of $BaTiO_3$ load on the dynamic responses ΔC of PHEMA-based sensors upon exposure to 5000 ppm of each one of the four vapor analytes. Frequency of measurements: 1 kHz. [Color figure can be viewed in the online issue, which is available at wileyonlinelibrary.com.]

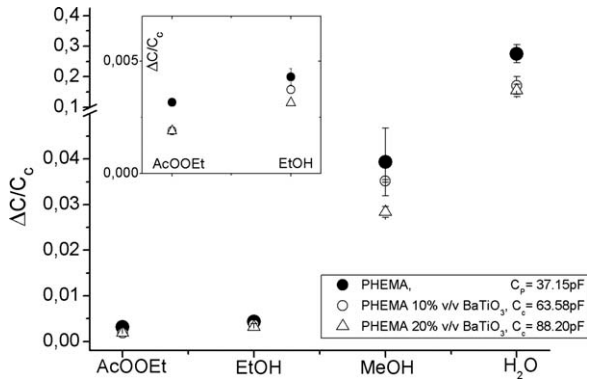

Figure 8 Effect of $BaTiO_3$ load on the equilibrium normalized responses $\Delta C/C_c$ of PHEMA-based sensors upon exposure to 5000 ppm of each one of the four vapor analytes. Error bars represent standard error of mean experimental values, derived from at least three samples. The data for AcOOEt and EtOH are also shown in the inset of the plot. Frequency of measurements: 1 kHz.

capacitance change induced by AcOOEt is attributed to both the low extend of sorption and the low ε_s of this compound ($\varepsilon_s = 6$). The increasingly higher responses as we move to EtOH and MeOH are attributed to the increasing sorptive capacity and polarity of the analyte ($\varepsilon_s = 24$ for EtOH and 32 for MeOH). Finally, the highest ΔC observed for H_2O at 5000 ppm is the result of both the high ε_s (=80) of water and the higher activity of water vapor resulting in enhanced amount of water sorbed.

In relation to the composite-based sensors, Figure 7 indicates that the response ΔC to each analyte increases with increasing amount of $BaTiO_3$ load, due to the increasing initial C_c values of the sensing layers. On the other hand, to evaluate the contribution of $BaTiO_3$ on the sensing properties of the composite layer, the normalized responses $\Delta C/C_c$ should also be considered. As shown in Figure 8, for each one of the four analytes, $\Delta C/C_c$ tends to be lower than the corresponding value of the pure PHEMA layer. These results indicate that the analyte-induced capacitance changes in the composite layers are mainly determined by sorption of the analyte in the polymer matrix. The implications of these results on other critical characteristics of sensor's performance can also be discussed. If we define the sensitivity of a sensor to a particular analyte as $S = (\Delta C/c_g)/C_p$ (where c_g is the vapor concentration in ppm),[27] then for each analyte depicted in Figure 8, the relative values of $\Delta C/C_c$ provide a comparison of the sensor's sensitivity at 5000 ppm. Thus, for all analytes, the sensitivity is decreasing with increasing $BaTiO_3$ content, but the extent of reduction is similar for all analytes, i.e., the selectivity of each sensor to pairs of analytes is practically unaltered by the presence of $BaTiO_3$ in the sensing layer.

Effect of $BaTiO_3$ load on the responses of PBMA-based sensors

The capacitance changes ΔC of a pure PBMA sensor, as well as of composite PBMA $-BaTiO_3$ sensors, upon exposure to 5000 ppm of each of the four analytes, are shown in Figure 9. The sorptive capacity of PBMA increases in the following order: H_2O<MeOH<EtOH< AcOOEt, with extremely low levels of sorption of H_2O.[26] In this case, due to the reverse order of ε_s, pure PBMA sensor exhibits a much lower differentiation towards the four analytes as compared with the pure PHEMA sensor, with responses ΔC moderately decreasing as we move from AcOOEt to H_2O.

As in the case of PHEMA-based composite sensors, with increasing amount of $BaTiO_3$ load, the response ΔC to each analyte is increased, but here the extend of ΔC enhancement is higher for H_2O, with the end result of similar responses to H_2O and AcOOEt for the higher $BaTiO_3$-loaded sensor (Fig. 9). In terms of normalized responses $\Delta C/C_c$ (Fig. 10) the behavior is similar to that of PHEMA-based sensors for AcOOEt, MeOH, and EtOH, i.e., with increasing $BaTiO_3$ load, $\Delta C/C_c$ of the composite layers is reduced as compared with the pure PBMA layer. However, in the case of H_2O the inverse behavior is observed, i.e., $\Delta C/C_c$ tend to be higher for the composites than for the pure PBMA.

Thus, with the exception of the PBMA-based composites in the presence of H_20, the normalized capacitance change is reduced with increasing $BaTiO_3$ load, as expected due to the decreasing volume fraction of the sorbing polymeric material. In contrast, water vapor effects in PBMA composites, indicates that the presence of $BaTiO_3$ affects the sorption, and consequently the dielectric, properties of the

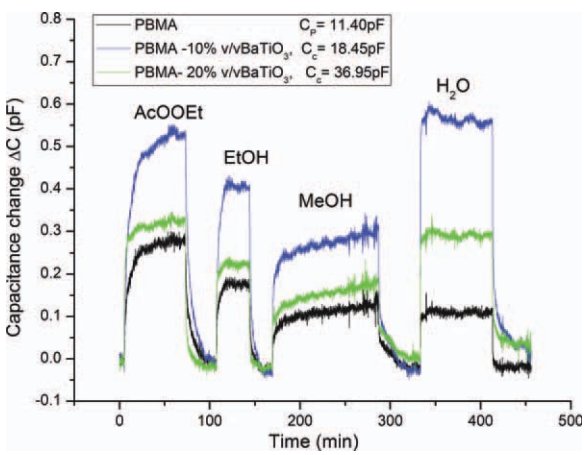

Figure 9 Effect of $BaTiO_3$ load on the dynamic responses ΔC of PBMA-based sensors upon exposure to 5000 ppm of each one of the four vapor analytes. Frequency of measurements: 1 kHz. [Color figure can be viewed in the online issue, which is available at wileyonlinelibrary.com.]

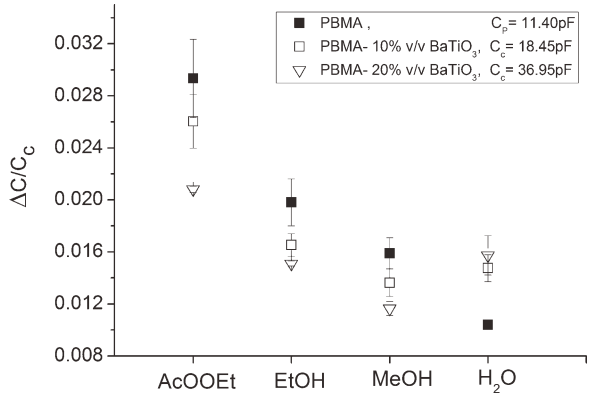

Figure 10 Effect of $BaTiO_3$ load on the equilibrium normalized responses $\Delta C/C_c$ of PBMA-based sensors upon exposure to 5000 ppm of each one of the four vapor analytes. Error bars represent standard error of mean experimental values, derived from at least three samples. Frequency of measurements: 1 kHz.

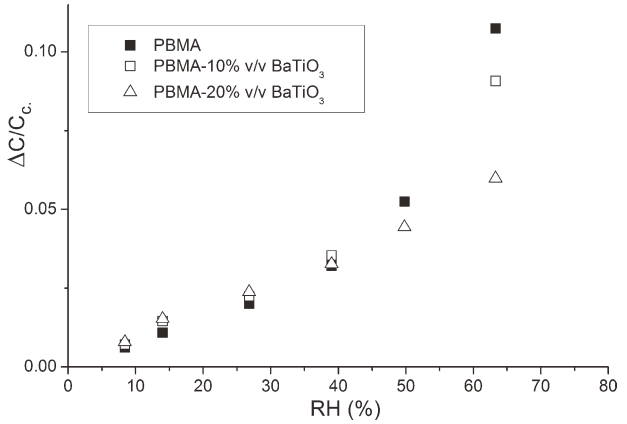

Figure 12 Normalized capacitance responses of PBMA-based sensors as a function of equilibrating relative humidity: pure PBMA [■], PBMA −10% v/v BaTiO3 (□) and PBMA −20% v/v $BaTiO_3$ (△). Frequency of measurements: 1 kHz.

composite layers. However similar effects were not discerned in the H_2O-PHEMA-based sensors.

To further investigate this behavior, we studied the responses of the sensors based on pure PBMA and pure PHEMA and on the corresponding composites loaded with 10%v/v and 20% v/v $BaTiO_3$ in a range of equilibrating relative humidity values (RH). The results are presented in Figures 11 and 12, as normalized responses $\Delta C/C_c$ versus RH. As shown in Figure 11, the behavior of the H_2O-PHEMA composites at 5000 ppm (corresponding RH ∼ 14%), shown in Figure 8, persists up to 70% RH. On the other hand, as shown in Figure 12, the behavior of the PBMA-based sensors at 14% RH (Fig. 10) tends to be reversed above 30%RH.

Theoretical treatments of sorption and diffusion phenomena (as well as of other analogous properties e.g., thermal and electrical conductivity, electrical permittivity, and elastic modulus) in heterogeneous composite materials take into account various parameters of the dispersed particle phase, such as shape, size, and size distribution, concentration, orientation and topology.[16,28] Moreover, in real situations, particle agglomerates and poor interfacial adhesion is likely to occur, especially in the case of glassy polymers,[29] resulting in voids formed at the polymer-particle interface. The effect on sorption properties is twofold. In the first place, analyte molecules may occupy the voids, and second, a larger fraction of unwetted agglomerate surface may be available for analyte adsorption.[16,28] Accordingly, the results of Figure 12 may be attributed to water molecules, adsorbed on the unwetted part of the $BaTiO_3$ particles surface,[9,10] when present in the hydrophobic PBMA environment, and contributing to the increase of the overall capacitance of the composite PBMA/$BaTiO_3$ layer. The effect ceases to be discernible above a certain humidity level, probably due to saturation of the available adsorption sites on the particles. Interestingly, evidence of similar phenomena were not detected in the case of PHEMA composites, although the larger $BaTiO_3$ aggregates observed in this case [Fig. 1(b)] in conjunction with the more rigid structure of glassy PHEMA, are expected to favor the formation of interfacial voids. The different behavior of the two types of composites studied here, upon exposure to low humidity levels is not completely clear at this moment, but may be partly due to the significantly higher hydrophilicity of PHEMA, as compared with PBMA one, which may mask any contribution of excess water adsorption due to the presence of the $BaTiO_3$ particles and to the fact that the observed larger particle aggregates in PHEMA [Fig. 1(b)], provide a lower surface density available for water molecules adsorption.

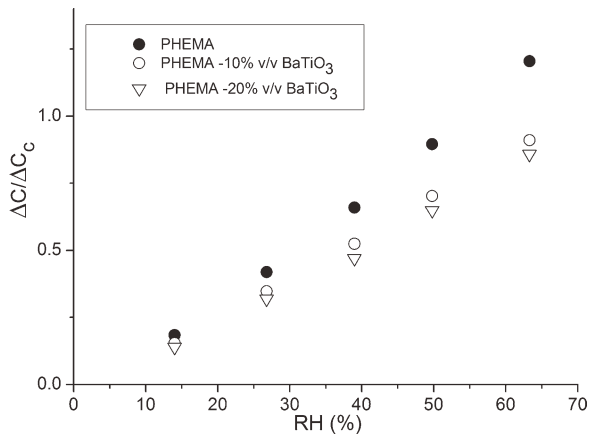

Figure 11 Normalized capacitance responses of PHEMA-based sensors as a function of equilibrating relative humidity: pure PHEMA [●], PHEMA-10% v/v $BaTiO_3$ (○) and PHEMA −20% v/v $BaTiO_3$ (▽). Frequency of measurements: 1 kHz.

CONCLUSIONS

The increase of the dielectric constant of the composites with increasing $BaTiO_3$ load, followed the Lichtenecker logarithmic mixing rule. However the effect was more intense in the case of PBMA than PHEMA, probably due to the better dispersion of barium titanate and the lower polarity of the polymer, in the former case. The same behavior was also observed for the initial capacitance values of chemocapacitors based on these composites. With increasing amount of $BaTiO_3$ load, the absolute value of response ΔC to 5000 ppm of four vapor analytes increased. However the corresponding normalized capacitance changes were reduced, indicating that $BaTiO_3$ is inert in respect to sorption. The extent of reduction was similar for all analytes, indicating that the selectivity of the sensors to pairs of these analytes was practically unaltered. An exception to this trend was observed upon exposure of the $BaTiO_3$/PBMA sensors to low humidity concentrations, indicating enhanced water effects in the presence of $BaTIO_3$ particles embedded in the PBMA environment.

References

1. Wenger, M. P.; Blanas, P.; Shuford, R. J.; Das-Gupta, D. K. Polym Eng Sci 1996, 36, 2945.
2. Tressler, J. F.; Alkoy, S.; Newnham, R. E. J Electroceram 1998, 2, 257.
3. Lynn, S. Y.; Newnham, R. E.; Klicker, K. A.; Rittenmyer, K.; Safari, A.; Schulze, W. A. Ferroelectrics 1981, 38, 955.
4. Xu, J.; Wong, C. P. J Appl Polym Sci 2007, 103, 1523.
5. Keller, P.; Ferkel, H.; Zweiacker, K.; Naser, J.; Meyer, J.-U.; Riehemann, W. Sens Act B 1999, 1–3, 39.
6. Wang, J; Xu, B. K.; Ruan, S. P.; Wang, S. P. Mater Chem Phys 2003, 78, 746.
7. Wang, J.; Xu, B.; Liu, G.; Zhang, J.; Zhang, T. Sens Act B 2000, 66, 159.
8. Wang, J.; Lin, Q.; Zhou, R.; Xu, B. Sens Act B 2002, 81, 248.
9. Caballero, A. C.; Villegas, M.; Fernandez, J. F.; Viviani, M.; Buscaglia, M. T.; Leoni, M. J Mater Sci Lett 1999, 18, 1297.
10. Wang, J.; Wang, X.-H.; Wang, X.-D. Sens Act B 2005, 108, 445.
11. De Girolamo del Mauro, A.; Ferrara, V. L.; Massera, E.; Miglietta, M. L.; Polichetti, T.; Rametta, G.; Francia, G. D. Macromol Symp 2009, 286, 203.
12. Dimopoulos, S.; Kitsara, M.; Goustouridis, D.; Chatzandroulis, S.; Raptis, I. Sensor Lett 2011, 9, 577.
13. Popielarz, R.; Chiang, C. K.; Nozaki, R.; Obrzut, J. Macromolecules 2001, 34, 5910.
14. Popielarz, R.; Chiang, C. K. Mater Sci Eng B 2007, 139, 48.
15. Kobayashi, Y.; Tanase, T.; Tabata, T.; Miwa, T.; Konno, M. J Eur Ceram Soc 2008, 28, 117.
16. Petropoulos, J. H. J Polym Sci: Polym Phys Ed 1985, 23, 1309.
17. Soulas, D.; Sanopoulou, M.; Papadokostaki, K. G. J Appl Polym Sci 2009, 113, 936.
18. Cho, S.-D.; Lee, S.-Y.; Hyun, J.-G.; Paik, K.-W. J Mater Sci Mater Electronics 2005, 16, 77.
19. Windlass, H.; Raj, P.; Balaraman, D.; Bhattacharya, S.; Tummala, R. IEEE Trans Adv Packaging 2003, 26, 10.
20. Kulek, J.; Szafraniak, I.; Hilczer, B.; Polomska, M. J Non-Crystalline Solids 2007, 353, 4448.
21. Kobayashi, Y.; Kosuge, A.; Konno, M. ApplSurface Sci 2008, 255, 2723.
22. Lim, E.-S.; Lee, J.-C.; Kim, J.-J.; Park, E.-T.; Chung, Y.-K.; Lee, H.-Y. Integrated Ferroelectrics 2005, 74, 53.
23. Casalini, R.; Nagel, J.; Oertel, U.; Petty, M. C. J Phys D: Appl Phys 1998, 31, 3146.
24. Casalini, R.; Kikitziraki, M.; Wood, D.; Petty, M. C. Sens Act B 1999, 56, 37.
25. Oikonomou, P.; Manoli, K.; Goustouridis, D.; Raptis, I.; Sanopoulou, M. Microelectronic Eng 2009, 86, 1286.
26. Manoli, K.; Goustouridis, D.; Raptis, I.; Valamontes, E.; Sanopoulou, M. J Appl Polym Sci 2010, 116, 184.
27. Zhou, R.; Hielermann, A.; Weimar, U.; Gopel, W. Sens Act B 1996, 34, 356.
28. Barrer, R. M. In Diffusion in Polymers; Crank, J.; Park, G. S., Eds., Academic Press: New York, 1968; Chapter 6.
29. Garcıa, M. G.; Marchese, J.; Ochoa, N. A. J Appl Polym Sci 2010, 118, 2417.